Agronomía Mesoamericana

Scientific article

Volumen 37: Artículo d981kg61, 2026
e-ISSN 2215-3608, https://doi.org/10.15517/d981kg61

Sorghum plant height and yield prediction using multispectral data and sUAS*

Predicción de altura de planta y rendimiento de sorgo mediante datos multiespectrales y VANT

Kevin Carrillo-Montoya[1], Jorge Claudio Vargas-Rojas[2], Melvin Lizano-Araya[3], Nevio Bonilla-Morales[4], Josselyne Aguilar López[5], José Roberto Camacho-Montero[1]

* Reception: August 18, 2025. Acceptance: January 19, 2026. This research forms part of the first author's master's thesis, entitled "Prediction of sorghum plant height and yield using multispectral data and RPAS photogrammetry" conducted within the Professional Master's Program in Geographic Information Systems and Remote Sensing at the University of Costa Rica.

1 Instituto Nacional de Innovación y Transferencia en Tecnología Agropecuaria. Mata Redonda, San José, Costa Rica. kevincarrillo029@gmail.com (corresponding author, https://orcid.org/0000-0003-0794-690X); rcamachom@inta.go.cr (https://orcid.org/0000-0001-8810-5437).

2 Universidad de Costa Rica, Sede Regional de Guanacaste. Liberia, Costa Rica. jorgeclaudio.vargas@ucr.ac.cr (https://orcid.org/0000-0002-1139-2148).

3 Universidad de Costa Rica, Escuela de Geografía. San José, Costa Rica. melvin.lizanoaraya@ucr.ac.cr (https://orcid.org/0000-0003-3437-3502).

4 Instituto Nacional de Innovación y Transferencia en Tecnología Agropecuaria, Centro de Innovación Enrique Jiménez Núñez. Cañas, Guanacaste, Costa Rica. nbonilla@inta.go.cr (https://orcid.org/0000-0001-6664-8377).

5 Independent researcher. Cañas, Guanacaste, Costa Rica. jaguilarlopez20@gmail.com (https://orcid.org/0009-0003-0066-3787).

Abstract

Introduction. The projected growth of the global population poses a significant challenge in ensuring sufficient food production. Crop genetic improvement, essential to meet this demand, relies on advanced technologies to accelerate field phenotyping processes. **Objective.** To predict plant height and biomass yield in sorghum using photogrammetry and multispectral data acquired through small unmanned aircraft system (sUAS) flights. **Materials and methods.** Six sorghum genotypes were evaluated in Cañas, Guanacaste, Costa Rica, using a completely randomized design with eight replications per genotype. Multispectral sensor flights were conducted at selected phenological stages to generate vegetation indices, digital terrain models (DTMs), and digital surface models (DSMs). Manual plant height measurements were used for correlation and simple linear regression analyses, while biomass was predicted using random forest regression. **Results.** The DTMs and DSMs enabled reliable estimation of plant height during early growth stage (R^2 = 0.53) and achieved higher accuracy at later stages (R^2= 0.76; RMSE = 0.13 m). Biomass prediction was most accurate at the booting stage (r= 0.72; RMSE = 1.40 t·ha^{-1}), with NDRE (Normalized Difference Red-Edge Index) and IKAW (Kawashima Index) identified as the most relevant spectral indices. **Conclusions.** The DTMs and DSMs derived from multispectral imagery accurately predicted plant height during later growth stages but were less accurate in early stages. Incorporating plant height alongside spectral indices into predictive models enhanced biomass yield prediction. The findings demonstrate that sUAS-mounted sensors and multispectral indices are valuable tools for phenotyping in sorghum breeding programs in Costa Rica.

Keywords: remote sensing, breeding, random forest regression, phenotyping.

Resumen

Introducción. El crecimiento proyectado de la población mundial representa un desafío significativo para garantizar una producción alimentaria suficiente. El mejoramiento genético de cultivos, esencial para satisfacer esta demanda, depende de tecnologías avanzadas para acelerar los procesos de fenotipado en campo. **Objetivo.** Predecir la altura de planta y el rendimiento de biomasa en sorgo utilizando fotogrametría y datos multiespectrales adquiridos mediante vuelos con pequeños vehículos aéreos no tripulados (VANT). **Materiales y métodos.** Se evaluaron seis genotipos de sorgo en Cañas, Guanacaste, Costa Rica, en un diseño completamente aleatorizado con ocho réplicas por genotipo. Se realizaron vuelos con un sensor multiespectral en etapas fenológicas seleccionadas para generar índices de vegetación, modelos digitales de terreno (MDT) y modelos digitales de superficie (MDS). Las mediciones manuales de la altura de la planta se utilizaron para análisis de correlación y regresión lineal simple; la biomasa se predijo mediante regresión con random forest. **Resultados.** Los MDT y los MDS proporcionaron una estimación confiable de la altura de la planta durante la etapa de crecimiento inicial ($R^2 = 0,53$) y alcanzaron una mayor precisión en etapas posteriores ($R^2 = 0,76$; RMSE = 0,13 m). La predicción de biomasa fue más precisa durante el estado de bota ($r = 0,72$; RMSE = 1,40 $t \cdot ha^{-1}$). Se identificaron el índice de diferencia normalizada del borde rojo y el índice de Kawashima como los espectrales más relevantes. **Conclusiones.** Los MDT y MDS derivados de imágenes multiespectrales predijeron con precisión la altura de planta en etapas posteriores de crecimiento, pero fueron menos precisos en etapas tempranas. La incorporación de la altura de la planta junto con los índices espectrales en los modelos mejoró la predicción de la biomasa. Los sensores montados en VANT y los índices multiespectrales son herramientas potenciales para el fenotipado en programas de mejoramiento de sorgo en Costa Rica.

Palabras clave: sensores remotos, mejoramiento, bosques aleatorios, fenotipado.

Introduction

Food security is essential for ensuring the well-being of the global population through access to safe and nutritious food. The United Nations estimates that the world population will reach 9.8 billion by 2050, posing significant challenges to agricultural sustainability and crop production (United Nations, 2017). Sorghum (*Sorghum bicolor* L. Moench) is a crop notable for its adaptability to adverse environmental conditions and its high nutritional value; it is also a strategic alternative to maize for both human and animal consumption in developing countries (Orozco Barrantes & Sánchez Ledezma, 2018). However, sorghum production faces global challenges, including climate change, degradation of natural resources, and competition for land use, which threaten both yields and food security, particularly in vulnerable regions (Hagen et al., 2022).

Crop breeding programs play a crucial role in addressing these challenges by developing new varieties with improved traits, such as higher yields, disease resistance, drought tolerance, and enhanced nutritional value (Aswini et al., 2023). Phenotyping, defined as the assessment of a plant's observable characteristics influenced by genetic and environmental factors, is a critical component of crop breeding programs, as it allows for the identification of superior genotypes with desirable traits (Aswini et al., 2023). However, traditional phenotyping methods present significant limitations in terms of cost, time efficiency, and accuracy (Hall & Richards, 2013; Watt et al., 2020).

Conventional phenotyping relies on destructive sampling and visual assessments to measure important traits such as biomass yield and plant height. These methods can pose logistical challenges in terms of cost and time

for genetic breeding programs (Mbaye et al., 2022). In recent years, while these approaches have been valuable, they can lead to human error, particularly in visual assessments, due to the large number of measurements required across diverse populations. These limitations delay the development of improved varieties and prolong the screening and release of lines suitable for agricultural production (Gano et al., 2021).

As a result of these limitations, several studies have explored alternative phenotyping methods, including the use of multispectral sensors mounted on small unmanned aircraft systems (sUAS) to accelerate field phenotyping, as demonstrated by Jiang et al. (2021) in rice, Ranđelović et al. (2023) in soybean, and Watanabe et al. (2017) in sorghum. These sensors can capture high spatial resolution imagery, enabling the monitoring of key crop traits (Shi et al., 2016; Yang et al., 2017). Moreover, vegetation indices can be calculated from radiometrically calibrated orthomosaics derived from sUAS imagery, such as the normalized difference red-edge (NDRE), which is commonly used to estimate biomass and stress levels in crops (Yang et al., 2017).

Furthermore, images acquired by these sensors can be processed using UAS-based photogrammetry to generate digital elevation models (DEMs), from which digital surface models (DSMs) and digital terrain models (DTMs) can be derived. These elevation products facilitate the estimation of crop growth by enabling the accurate detection of morphological changes and continuous monitoring of crop development (Malambo et al., 2018). Promising results have been reported in Costa Rica by Alemán Montes et al. (2021), who successfully predicted sugarcane yield using sUAS-derived DSMs and DTMs, achieving more accurate predictions three months before harvest.

Similarly, outside Costa Rica, Stavrakoudis et al. (2019) reported a strong correlation ($R^2 = 0.80$) between sUAS-derived vegetation indices and rice biomass. In wheat, Yue et al. (2017) improved biomass prediction accuracy ($R^2 = 0.74$) by integrating plant height with vegetation indices such as the NDVI (normalized difference vegetation index), the enhanced vegetation index (EVI), and the ratio vegetation index (RVI). These findings underscore the potential of sUAS-based phenotyping in sorghum breeding programs, offering a rapid and accurate approach for trait assessment under diverse environmental conditions (Araus & Kefauver, 2018; Chivasa et al., 2020).

Despite the growing adoption of sUAS-based phenotyping, its application in sorghum breeding programs under tropical conditions remains largely underexplored. Previous research has primarily focused on other crops such as wheat, rice, and maize across various latitudes, leaving a critical gap in understanding how remote sensing technologies can improve sorghum biomass prediction and plant height monitoring for genotype selection in local breeding programs. In this context, the objective of this study was to predict plant height and biomass yield in sorghum using photogrammetry and multispectral data acquired through small unmanned aircraft system (sUAS) flights.

Materials and methods

Location

The study was carried out at the Enrique Jiménez Núñez Research Center of the National Institute of Agricultural Technology (INTA) of Costa Rica in the Guanacaste province (Figure 1). The site is located at 10° 20’ 39.73” N and –85° 08’ 8.62” W, with an elevation of 14 m above sea level. The region, classified as a Premontane Humid Forest life zone, experiences temperatures ranging from 22 to 33 °C and receives an annual precipitation between 1500 and 1900 mm (Instituto Meteorológico Nacional, 2023).

Genetic material and experimental design

The experiment was conducted from September to December 2023, evaluating six sorghum genotypes: BMR-0936, PCR-3-22, CENTA CF, CENTA RCY, Sureño, and a local cultivar commonly known as “sorgo negro”

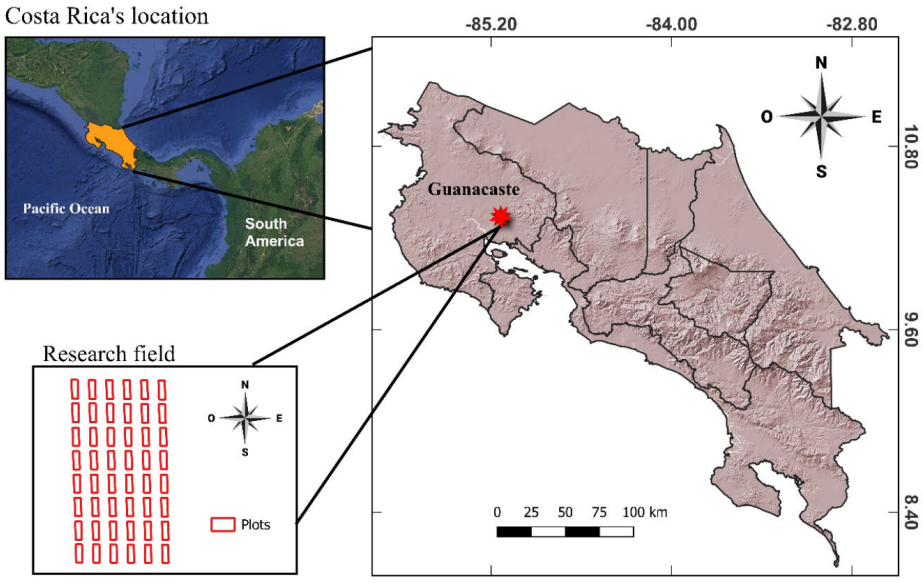

Figure 1. Experimental site and field plots at Enrique Jiménez Núñez Research Center. Cañas, Guanacaste. 2023.

Figura 1. Sitio experimental y parcelas de campo en el Centro de Investigación Enrique Jiménez Núñez. Cañas, Guanacaste. 2023.

(*Sorghum almum*), which is widely grown by farmers across the country. A total of 48 experimental units were established using a completely randomized design, with eight replications per genotype. Each experimental unit consisted of four rows, each five meters in length and spaced 70 cm apart. To minimize border effect, a 120 cm separation was maintained between plots. The soil in the experimental area is classified as Mollisol order, with a clay-loam texture, slightly alkaline pH, with available concentrations of Ca, Mg, P, Fe and Cu, and showed Zn and K values slightly below the critical level (Table 1), which were considered for nutritional adjustment.

Table 1. Soil fertility indicators obtained in the experimental area. Enrique Jiménez Núñez Experimental Innovation Center, Cañas, Guanacaste. 2023.

Cuadro 1. Parámetros de fertilidad del suelo obtenidos en área experimental. Centro de Innovación Enrique Jiménez Núñez, Cañas, Guanacaste. 2023.

KCl-Modified Olsen	pH H_2O	Acidity	cmol(+) L^{-1}			%		mg L^{-1}				
			Ca	Mg	K	ECEC	AS	P	Zn	Cu	Fe	Mn
Critical level	5.50	0.50	4.00	1.00	0.20	5.00	10	10.00	3.00	1.00	10.00	5.00
Soil	6.60	0.15	12.40	4.40	0.12	16.92	0.90	13.00	2.80	19.90	206.50	10.50

pH H_2O: Soil pH measured in water. **ECEC:** Effective cation exchange capacity. **AS:** aluminum saturation. / **pH H_2O:** pH del suelo medido en agua. **ECEC:** Capacidad de intercambio catiónico efectiva. **AS:** Saturación de aluminio.

UAS data acquisition

Field control markers were initially established, and five ground control points (GCPs) were georeferenced using a GEOMAX Zenith40 geodetic receiver station. A flight plan was designed using the DJI Pilot Application

and a 50-meter buffer around the experiment perimeter was defined to ensure proper data acquisition. Multispectral data were collected using a MicaSense Altum 05 sensor mounted on a DJI Matrice 210 multirotor sUAS. The sensor captured data in narrow spectral bands: blue (475 nm ± 32 nm), green (560 nm ± 27 nm), red (668 nm ± 14 nm), red-edge (717 nm ± 12 nm) and near-infrared (NIR; 842 nm ± 57 nm). Although the sensor is equipped with a thermal long-wave infrared band (11 μm ± 57 μm), thermal imagery was not used in the present study.

The sUAS operated autonomously following predefined flight parameters. Flights were conducted at a speed of 10.8 km/h, with 80 % lateral and frontal overlap, and an altitude of 45 m, achieving an average ground sampling distance (GSD) of 2.04 cm/pixel. Data collection was performed during distinct crop phenological stages (Table 2) between 11:00 and 12:00 hours under clear, sunny conditions to ensure optimal illumination. Additionally, images of a calibrated reflectance panel were captured before and after each flight to enable radiometric calibration of the multispectral data.

Table 2. Climatic conditions and purpose of each flight during the different phenological stages of sorghum. Cañas, Guanacaste. 2023.

Cuadro 2. Condiciones climáticas y propósito de cada vuelo durante las diferentes etapas fenológicas del sorgo. Cañas, Guanacaste. 2023.

Phenological stage	DAS (days after sowing)	Image use	Average temperature (°C)	Average wind speed (km/h)
----------	0	DTM	30.2	6.4
Visible flag leaf	42	Multispectral + DSM	30.0	1.6
Booting	56	Multispectral	31.9	8.0
Flowering	62	Multispectral	32.1	12.9
Milky grain	74	Multispectral	34.5	11.3
Dough grain	83	Multispectral + DSM	31.0	12.9

Field measurement of plant height

Plant height measurements were taken at two different times. At 42 DAS (visible flag leaf stage), the measurement was taken from the base of the stem to the most exposed leaf surface (Figure 2A), while at 83 DAS (dough grain stage), the measurement was taken from the same reference point to the panicle apex (Figure 2B), depending on the phenological stage. Eight plants were randomly selected from the inner rows of each plot to minimize border effects.

Biomass

All plants within a two-meter linear segment of the central rows of each plot were harvested at ground level on 23 December 2023. The total fresh biomass was measured using an electronic balance (Ocony SS). Approximately 500 g of a homogenized biomass sample was collected and placed in a labelled plastic bag for transportation to the laboratory. The samples were dried in a forced-air circulation oven at 60 °C for 72 hours. A portion of the dried sample was then placed in an oven at 105 °C to determine the total dry biomass.

Figure 2. Description of field sorghum plant height measurements. A) Exposed leaf. B) Panicle apex. Cañas, Guanacaste. 2023.

Figura 2. Descripción de la medición de altura de la planta de sorgo en campo. A) Hoja expuesta. B) Panoja. Cañas, Guanacaste. 2023.

Multispectral photogrammetric process

Ground control points were processed using the online platform of the Leica Spider Business Center module, operated by the National Geographic Institute of Costa Rica. All captured images were imported into Pix4Dmapper, version 4.7.5 (Pix4D S.A., Lausanne, Switzerland), and the workflow specifically designed for multispectral image processing was applied. The initial step consisted of identifying matching keypoints, followed by camera localization, orientation, and optimization (Pix4D, 2017).

The resulting georeferenced GCPs were subsequently integrated into Pix4Dmapper following the initial processing step. Each GCP was manually identified in at least four images corresponding to the field control markers. The automatic adjustment process was then run, and the project was further optimized. The workflow proceeded to the second step, where automatic tie points were generated, resulting in a dense georeferenced point cloud. From this point cloud, a textured 3D mesh was constructed (Figure 3).

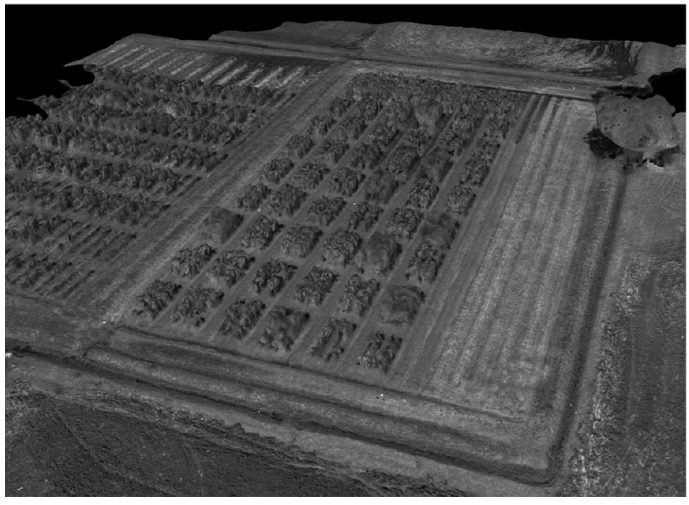

Figure 3. Three-dimensional mesh of the experimental plots generated from UAS imagery using Pix4D. Cañas, Guanacaste. 2023.

Figura 3. Malla tridimensional de las parcelas experimentales generada a partir de imágenes UAS mediante Pix4D. Cañas, Guanacaste. 2023.

Radiometric calibration and derived products

The calibration panel images were automatically recognized by the software and the panel calibration option in Pix4Dmapper was selected, verifying the reflectance values for each spectral band value. Finally, three main products were derived in the third processing step: the digital terrain model (DTM), the digital surface model (DSM), and the orthomosaics. For the DSM, the inverse distance weighted interpolation method was applied. The DTM resolution was set to five times the final GSD, as recommended by Pix4Dmapper. Furthermore, the spatial resolutions of the generated products (orthophotos and models) were defined during the export process to ensure consistency across products from different flights. In addition, 17 vegetation indices (VI) that have been used to estimate biophysical parameters in previous studies were calculated, as shown in Table 3.

Table 3. Vegetation indices used in the study. R: red; G: green; B: blue; RE: red-edge; and NIR: near-infrared. Cañas, Guanacaste. 2023.

Cuadro 3. Índices de vegetación utilizados en el estudio. R: rojo; G: verde, B: azul, RE: borde rojo y NIR: infrarrojo cercano, Cañas, Guanacaste. 2023.

Index	Equation	Reference
BCC	B/ (R + G + B)	De Swaef et al. (2021)
CARI	RE / R	Ballester et al. (2019)
CIRE	(NIR / RE) – 1	Wan et al. (2020)
CVI	NIR (R / G^2)	Peroni Venancio et al. (2020)
DVI	NIR – R	Yang et al. (2017)
GCI	(NIR / G) – 1	Mandal et al. (2022)
GLI	(2G – R – B) / (2G + R + B)	Louhaichi et al. (2001)
GNDVI	(NIR – G) / (NIR + G)	Gitelson et al. (1996)
IKAW	(R – B) / (R + B)	Kawashima & Nakatani (1998)
NDRE	(NIR – RE) / (NIR + RE)	Marques Ramos et al. (2020)
NDVI	(NIR – R) / (NIR + R)	Rouse et al. (1974)
RCC	R / (R + G + B)	De Swaef et al. (2021)
RDVI	(NIR – R) / √ (NIR + R)	Roujean and Breon (1995)
REDVI	NIR – RE	Kanke et al. (2016)
RGRI	R / G	Tayade et al. (2022)
SAVI	1.5 (NIR – R) / (NIR + R + 0.5)	Huete (1988)
SR	NIR / R	Jordan (1969)

BCC: blue chromatic coordinate index. **CARI:** chlorophyll absorption ratio index. **CIRE:** chlorophyll index red edge. **CVI:** chlorophyll vegetation index. **DVI:** difference vegetation index. **GCI:** green chlorophyll index; GLI: green leaf index. **GNDVI:** green normalized difference vegetation index; **IKAW:** Kawashima index. **NDRE:** normalized difference red-edge index. **NDVI:** normalized difference vegetation index; **RCC:** red chromatic coordinate index. **RDVI:** renormalized difference vegetation index. **REDVI:** red edge difference vegetation index; **RGRI:** red–green ratio index; **SAVI:** soil adjusted vegetation index. **SR:** simple ratio index. / **BCC:** índice de coordenada cromática azul. **CARI:** índice de razón de absorción de clorofila. **CIRE:** índice de clorofila borde rojo. **CVI:** índice de vegetación de clorofila. **DVI:** índice de diferencia de vegetación.**GCI:** índice de clorofila verde. **GLI:** índice de hoja verde. **GNDVI:** índice de vegetación de diferencia normalizada verde. **IKAW:** índice de Kawashima. NDRE: índice de diferencia normalizada del borde rojo. **NDVI:** índice de vegetación de diferencia normalizada. **RCC:** índice de coordenada cromática roja. **RDVI:** índice de vegetación de diferencia renormalizada. **REDVI:** índice de vegetación de diferencia del borde rojo. RGRI: índice de razón rojo verde. **SAVI:** índice de vegetación ajustado al suelo. **SR:** índice de relación simple.

ISSN 2215-3608 https://doi.org/10.15517/d981kg61

Extracting soil, plant canopy and multispectral values

A geospatial analysis workflow, as described by Matias et al. (2020), was employed for vector-based plot delineation and soil segmentation. Following this process, the segmented vector layer containing the delineated plots was used to extract structural features, specifically the DTM and DSM. Sorghum plant height was subsequently calculated as the difference between the mean DSM and DTM values for each plot, as shown in equation 1. Furthermore, the mean values of spectral bands and vegetation indices (VI) from all flight datasets were also extracted based on the plot delineation and segmentation methodology described above.

Plant height = Mean pixels (DSM) – Mean pixels (DTM) (1)

Statistical analysis

Correlation and simple linear regression analyses were applied to assess the relationship between measured plant height and plant height obtained through the photogrammetric process. All these analyses were carried out using Navure software, version 2.7.1 (Navure Team, n. d.).

In addition, multitemporal correlation analyses were conducted between UAS-derived spectral indices at each phenological stage and sorghum biomass. Spectral indices showing correlation coefficients greater than 0.50 were selected, together with sensor-derived plant height, as predictor variables for biomass prediction using a random forest (RF) regression model.

Given the relatively small dataset, the data were randomly partitioned into 70 % for model training and 30 % for validation. Models were built using the regressoR package developed by Rodriguez (2023) within the R statistical software environment, version 4.4.3 (R Core Team, 2020). RF models were fitted using the default hyperparameter settings of the regressoR package, with a sufficiently large number of trees to ensure model stability. Model performance was evaluated using the correlation between observed and predicted values and the root mean square error (RMSE). Variable importance was assessed only for the best-performing RF model using an error-based (permutation) approach, quantified as the increase in prediction error based on the mean squared error (MSE) when each predictor was permuted while keeping all other variables unchanged. All formulas are provided in equations 2-4.

$$R^2 = 1 - \frac{\sum_{i=1}^{n}(yi - \hat{y}i)^2}{\sum_{i=1}^{n}(yi - \bar{y}i)^2} \quad (2)$$

$$\mathrm{RMSE} = \sqrt{\frac{1}{n}\sum_{i=1}^{n}(yi - \hat{y}i)^2} \quad (3)$$

$$\mathrm{MSE} = \frac{1}{n}\sum_{i=1}^{n}(yi - \hat{y}i)^2 \quad (4)$$

Where n is the number of samples in the model; yi is the actual measured value; $\bar{y}i$ is the mean of the measured values; and $\hat{y}i$ represents the predicted value.

ISSN 2215-3608 https://doi.org/10.15517/d981kg61

Results

Plant height

The measured plant height at 42 DAS ranged between 0.20 m and 1.06 m (mean = 0.55 m and SE = 0.03 m) (Figure 4A). At 83 DAS, plant height ranged from 1.32 m to 2.54 m (mean = 1.83 m and SE = 0.04 m) (Figure 4B). The results indicated a strong relationship between manual and sensor-estimated measurements, with correlation coefficients of r = 0.74 and r = 0.88 at 42 and 83 DAS, respectively (Figure 4). When this relationship was assessed using simple linear regression analysis, the model fit was moderate at 42 DAS (R^2 = 0.53; RMSE = 0.12 m), and improved at 83 DAS (R^2 = 0.76; RMSE = 0.13 m).

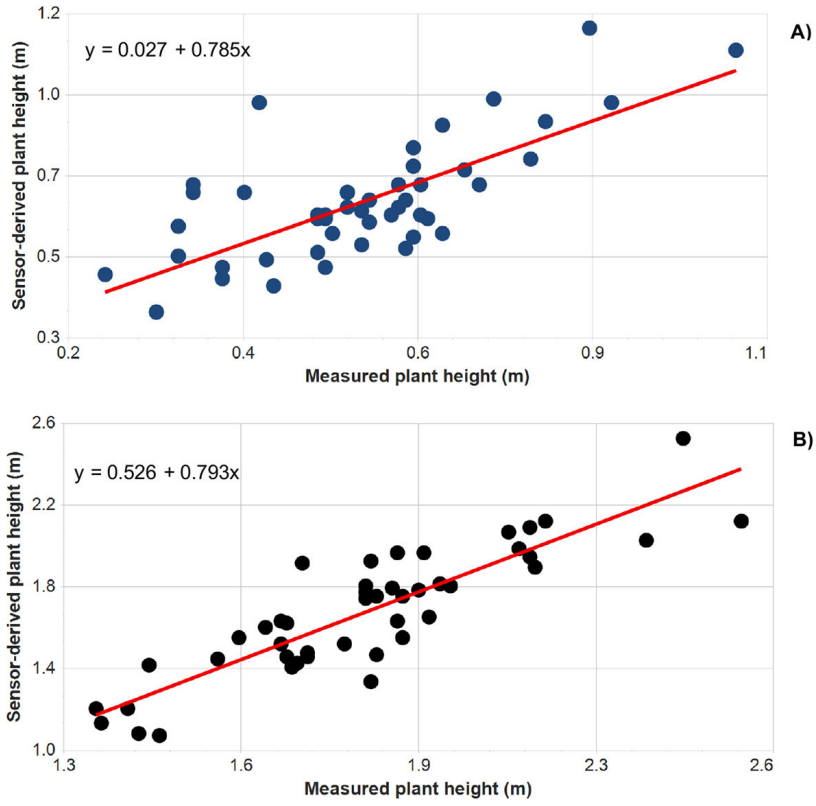

Figure 4. Scatter plot between manually measured plant height and sensor-derived plant height at different days after planting (DAS). A) 42 DAS. B) 83 DAS. Cañas, Guanacaste. 2023.

Figura 4. Diagrama de dispersión entre la altura de la planta medida manualmente y la altura de la planta derivada del sensor en diferentes días después de la siembra (DDS). A) 42 DDS. B) 83 DDS. Cañas, Guanacaste. 2023.

Biomass yield

The Spearman correlation between sorghum biomass yield and vegetation indices varied across phenological stages. During the visible flag leaf stage, several indices showed moderate correlations with biomass, including GNDVI ($r = 0.51$), GCI ($r = 0.49$), CIRE ($r = 0.45$), and NDRE ($r = 0.45$). During the booting and flowering stages, correlation coefficients for several indices increased. IKAW showed a relatively strong negative correlation at the booting stage ($r = –0.70$), while NDRE ($r = 0.59$ and 0.58), and CIRE ($r = 0.58$ at both stages) exhibited moderate correlations with biomass yield. In contrast, correlations decreased during the milky grain and dough grain stages, and at the latter stage, most values were low or not statistically significant (Table 4).

Table 4. Spearman correlation between spectral indices and biomass yield during phenological stages. Cañas, Guanacaste. 2023.

Cuadro 4. Correlación de Spearman entre índices espectrales y rendimiento de biomasa durante etapas fenológicas. Cañas, Guanacaste. 2023.

Indice	Visible flag leaf	Booting	Flowering	Milky grain	Dough grain
BCC	0.43**	0.53**	0.40**	0.31*	0.31*
CARI	0.06	–0.01	0.08	0.32*	0.14
CIRE	0.45**	0.58**	0.58**	0.38**	0.26
CVI	0.47*	0.52**	0.47**	0.20	0.27
DVI	0.20	0.46**	0.29	0.22	0.16
GCI	0.49**	0.56**	0.54**	0.42**	0.32*
GLI	–0.16	–0.17	0.02	0.21	0.07
GNDVI	0.51**	0.57**	0.56**	0.46**	0.38**
IKAW	–0.38**	–0.70**	–0.55**	–0.45**	–0.24
NDRE	0.45**	0.59**	0.58**	0.43**	0.28
NDVI	0.36*	0.43**	0.45**	0.43**	0.25
RCC	0.01	–0.06	–0.32*	–0.32*	–0.12
RDVI	0.22	0.47**	0.33*	0.26	0.21
REDVI	0.24	0.51**	0.36*	0.22	0.17
RGRI	0.08	0.03	–0.23	–0.31*	–0.14
SAVI	0.24	0.47**	0.32*	0.26	0.22
SR	0.33**	0.38**	0.38**	0.29	0.22

*$p < 0.05$; **$p < 0.01$.

Although most correlations between spectral indices and biomass yield were not significant during the late stages of the crop cycle, a significant Pearson correlation ($r = 0.60$) was observed between sensor-derived plant height at 83 DAS and biomass yield (Figure 5). Based on this finding, plant height at 83 DAS was included as a predictor variable in random forest (RF) regression models developed for selected phenological stages to predict sorghum biomass yield, using vegetation indices alone and in combination with plant height.

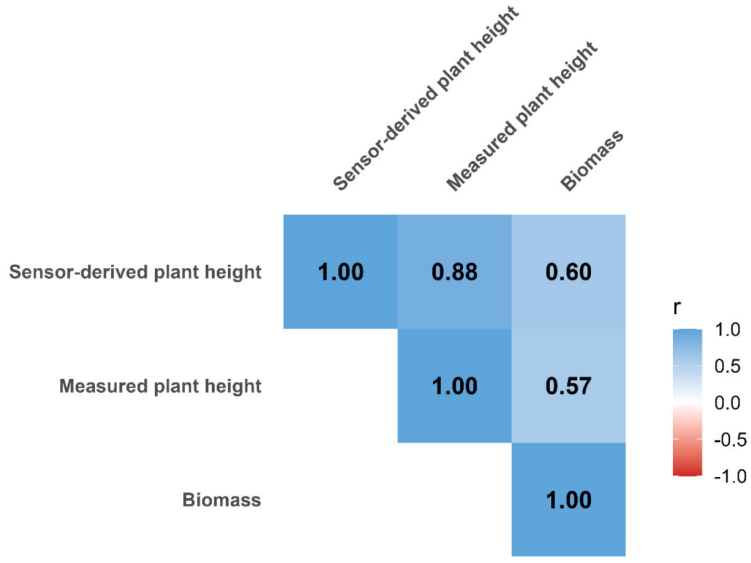

Figure 5. Pearson correlation matrix between sorghum measured plant height, sensor-derived plant height and sorghum biomass yield. Cañas, Guanacaste. 2023.

Figura 5. Matriz de correlación de Pearson entre la altura de la planta medida, la altura de planta derivada del sensor y el rendimiento de biomasa de sorgo. Cañas, Guanacaste. 2023.

The predictive performance of the RF models, evaluated using the correlation between predicted and observed values and RMSE, varied across phenological stages, with correlation coefficients ranging from r = 0.42 to r = 0.72, and RMSE values ranging from 1.40 to 2.20 t·ha^{-1} (Table 5). Incorporating sensor-derived plant height as an additional predictor alongside vegetation indices consistently improved the performance of all models, increasing the correlation by 0.12 to 0.20 units and reducing RMSE values by 0.11 to 0.59 t·ha^{-1} across phenological stages. While the flowering and milky grain stages exhibited improved accuracy with the addition of structural information, their predictive accuracy remained below that achieved at the booting stage. The RF model combining vegetation indices and sensor-derived plant height at booting achieved the highest predictive performance, reducing the RMSE by 0.33 t·ha^{-1} and increasing the correlation to r = 0.72 (Table 5).

Table 5. Predicted models for sorghum dry biomass based on phenological stages. Cañas, Guanacaste. 2023.

Cuadro 5. Modelos predichos para la biomasa seca del sorgo en función de etapas fenológicas. Cañas, Guanacaste. 2023.

Model	DAS	Phenological Stage	Variables	Correlation	RMSE
1	56	Booting	Only VI	0.60	1.73
2			VI + Sensor plant height	0.72	1.40
3	62	Flowering	Only VI	0.49	2.20
4			VI + Sensor plant height	0.63	1.61
5	74	Milky grain	Only VI	0.42	1.64
6			VI + Sensor plant height	0.62	1.53

Additionally, variable importance was assessed for the best-performing RF model (Model 2), which incorporated vegetation indices and sensor-derived plant height. The results indicated that sensor-derived plant height was the most influential predictor of biomass compared to the spectral indices (Figure 6). Among the vegetation indices, IKAW, NDRE, and BCC were identified as the most important, based on their percentage contribution to the increase in mean squared error (MSE).

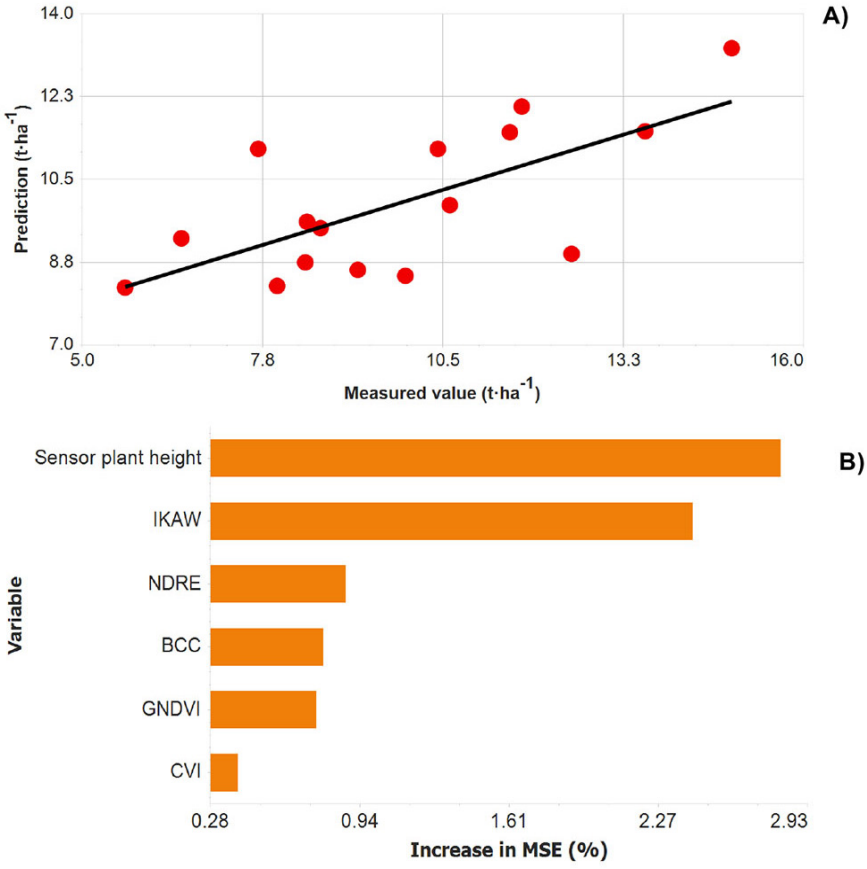

Figure 6. A) Observed versus predicted dry biomass based on the best-performing random forest model using spectral indices and photogrammetric plant height. **B)** Variable importance for Model 2. Cañas, Guanacaste. 2023.

Figura 6. A) Biomasa seca observada versus predicha con base en el modelo de random forest de mejor desempeño, utilizando índices espectrales y altura de planta fotogramétrica. **B)** Importancia de las variables en el modelo 2. Cañas, Guanacaste. 2023.

Discussion

The correlation between measured plant height and sensor-derived height at 42 DAS was strong (r = 0.74), while a higher correlation was observed at 83 DAS (r = 0.88). These results are consistent with those of Malambo et al. (2018), who reported correlations exceeding 0.80 between field-measured plant height and sensor-derived height from sUAS in sorghum. Similarly, Shu et al. (2023) observed strong correlations when combining growth stages but noted increased estimation errors as the crop advanced through its development. The authors attributed

these errors to inaccuracies in DTM generation caused by increased crop canopy coverage. In the present study, such errors were minimized by generating the DTM prior to crop establishment.

Plant height measurements during early growth stages are critical for understanding genotype responses to environmental conditions (Griffiths et al., 2012). The relatively lower correlation observed between manually measured and sensor-derived heights at 42 DAS is likely associated with the inclusion of soil data in the digital surface model during segmentation and subsequent pixel extraction. This methodological limitation may result in over- or underestimation of canopy elevation, as noted by Hassan et al. (2019).

Despite the expected increase in leaf area and the incorporation of ground control points (GCPs), the RMSE between predicted and measured plant height at 83 DAS was 13.0 cm. This deviation is likely associated with two main factors. First, wind-induced movement of the sorghum canopy can reduce image acquisition quality and compromise the identification of matching points during photogrammetric processing (Mesas-Carrascosa et al., 2015). Second, and more likely given the high positional accuracy achieved with GCPs, is the variability in leaf angles and canopy structure among the manually sampled genotypes. These structural differences affect the consistency between manual and sensor-derived measurements (Li et al., 2018).

Spectral indices have been widely recognized as relevant predictors of biomass in various annual crops such as wheat and rice (Jiang et al., 2019; Yue et al., 2017). In this study, the integration of crop height with spectral index values improved model accuracy across different phenological stages within the random forest framework. Similar findings were reported by Varela et al. (2021) in sorghum, where geometric information was identified as one of the most important biomass predictors, regardless of phenological stage. In barley, Bendig et al. (2015) demonstrated that combining plant height derived from surface models with spectral values also improved biomass prediction accuracy.

The Normalized Difference Red-Edge Index (NDRE) shares the effectiveness of NDVI as an indicator of crop nitrogen content (Fitzgerald et al., 2006). However, the replacement of the red band with the red-edge band in its calculation enhances NDRE's sensitivity to biomass variations, particularly during growth stages characterized by maximum foliar area. This heightened sensitivity is attributed to the strong energy absorption in the red-edge spectrum caused by chlorophyll content. As plants transition into senescence, reflectance in the red-edge band increases due to a decline in chlorophyll content (Xie et al., 2018). The findings of this study regarding red-edge-based indices are consistent with those of Cheng et al. (2017) in rice, who highlighted the strong association between red-edge-based vegetation indices and leaf biomass dominance.

The present study identified the IKAW index as an effective indicator for biomass estimation using RGB-based information. Previous studies have similarly highlighted the potential of RGB-based vegetation indices for biomass modeling. For instance, Bendig et al. (2014) demonstrated higher biomass estimation accuracy at early growth stages using visible-band indices, while Li et al. (2018) reported moderate correlations (r = 0.57) between dry biomass and the RGB vegetation index (RGBVI). The use of RGB-based approaches has the potential to significantly reduce costs, as sensors capturing visible-spectrum data are more affordable compared to those equipped with additional spectral bands.

Biomass prediction was most accurate during the booting stage, a critical growth phase when the plant reaches maximum leaf area and accumulates approximately 60% of its total dry matter (Gerik et al., 2003). This pattern is consistent with the findings by Zheng et al. (2018), where biomass predictions using multispectral indices were significantly more accurate prior to the R3 stage in rice compared to later stages. Furthermore, most vegetation indices selected in this study exhibited reduced prediction accuracy after the flowering stage due to biomass saturation, which limits index sensitivity. Additional factors contributing to this reduction include the reallocation of assimilates from leaves and stems to grains, complicate biomass predictions in advanced growth stages (Zheng et al., 2018).

Conclusions

This study demonstrates that sorghum plant height can be accurately predicted from digital terrain and surface models derived from multispectral images, particularly during later development stages. Early growth stages showed lower correlations, likely due to canopy variability between manual measurements and sensor-derived estimates.

Vegetation indices incorporating the near-infrared (NIR) and red-edge bands, as well as the IKAW index, were strongly correlated with dry biomass yield. Including sensor-derived plant height as a predictor variable in predictive models significantly improved model accuracy. The booting stage was identified as optimal for dry biomass predictions.

These results support the use of remote sensing technologies to enhance agronomic trait evaluation. Further research incorporating larger datasets is recommended to improve the broader applicability of this technology in breeding programs.

Acknowledgement

The authors would like to acknowledge the support of the Central American and Caribbean Crop Improvement Alliance (CACCIA) at INTA and the Feed the Future Innovation Lab for Crop Improvement (ILCI) at Cornell University, funded by the United States Agency for International Development (USAID), for their academic and technical collaboration during the development of this work. The authors gratefully acknowledge the technicians at INTA Costa Rica for their collaboration in field data collection and sample analyses.

Conflict of interests

The authors declare that there is no conflict of interest.

References

Alemán Montes, B., Henríquez Henríquez, C., Ramírez Rodríguez, T., & Largaespada Zelaya, K. (2021). Estimación de rendimiento en el cultivo de caña de azúcar (*Saccharum officinarum*) a partir de fotogrametría con vehículos aéreos no tripulados (VANT). *Agronomía Costarricense, 45*(1), 67-80. https://doi.org/10.15517/rac.v45i1.45695

Araus, J. L., & Kefauver, S. C. (2018). Breeding to adapt agriculture to climate change: affordable phenotyping solutions. *Current Opinion in Plant Biology, 45*, 237-247. https://doi.org/10.1016/j.pbi.2018.05.003

Aswini M. S., Kiran, Lenka, B., Shaniware , Y. A., Pandey , P., Dash , A. P., & Haokip , S. W. (2023). The role of genetics and plant breeding for crop improvement: Current progress and future prospects. *International Journal of Plant & Soil Science, 35*(20), 190-202. https://doi.org/10.9734/ijpss/2023/v35i203798

Ballester, C., Brinkhoff, J., Quayle, W. C., & Hornbuckle, J. (2019). Monitoring the effects of water stress in cotton using the green red vegetation index and red edge ratio. *Remote Sensing, 11*(7), Article 873. https://doi.org/10.3390/RS11070873

Bendig, J., Bolten, A., Bennertz, S., Broscheit, J., Eichfuss, S., & Bareth, G. (2014). Estimating biomass of barley using crop surface models (CSMs) derived from UAV-based RGB imaging. *Remote Sensing, 6*(11), 10395-10412. https://doi.org/10.3390/rs61110395

Bendig, J., Yu, K., Aasen, H., Bolten, A., Bennertz, S., Broscheit, J., Gnyp, M. L., & Bareth, G. (2015). Combining UAV-based plant height from crop surface models, visible, and near infrared vegetation indices for biomass monitoring in barley. *International Journal of Applied Earth Observation and Geoinformation, 39*, 79-87. https://doi.org/10.1016/j.jag.2015.02.012

Cheng, T., Song, R., Li, D., Zhou, K., Zheng, H., Yao, X., Tian, Y., Cao, W., & Zhu, Y. (2017). Spectroscopic estimation of biomass in canopy components of paddy rice using dry matter and chlorophyll indices. *Remote Sensing, 9*(4), Article 319. https://doi.org/10.3390/rs9040319

Chivasa, W., Mutanga, O., & Biradar, C. (2020). UAV-Based Multispectral Phenotyping for Disease Resistance to Accelerate Crop Improvement under Changing Climate Conditions. *Remote Sensing, 12*(15), Article 2445. https://doi.org/10.3390/rs12152445

De Swaef, T., Maes, W. H., Aper, J., Baert, J., Cougnon, M., Reheul, D., Steppe, K., Roldán-Ruiz, I., & Lootens, P. (2021). Applying RGB- and thermal-based vegetation indices from UAVs for high-throughput field phenotyping of drought tolerance in forage grasses. *Remote Sensing, 13*(1), Article 147. https://doi.org/10.3390/rs13010147

Fitzgerald, G. J., Rodriguez, D., Christensen, L. K., Belford, R., Sadras, V. O., & Clarke, T. R. (2006). Spectral and thermal sensing for nitrogen and water status in rainfed and irrigated wheat environments. *Precision Agriculture, 7*(4), 233-248. https://doi.org/10.1007/s11119-006-9011-z

Gano, B., Dembele, J. S. B., Ndour, A., Luquet, D., Beurier, G., Diouf, D., & Audebert, A. (2021). Using UAV borne, multi-spectral imaging for the field phenotyping of shoot biomass, leaf area index and height of West African sorghum varieties under two contrasted water conditions. *Agronomy, 11*(5), Article 850. https://doi.org/10.3390/agronomy11050850

Gerik, T., Bean, B., & Vanderlip, R. (2003). *Sorghum growth and development*. Texas A&M AgriLife Soil and Crop Science Department. https://hdl.handle.net/1969.1/202690

Gitelson, A. A., Kaufman, Y. J., & Merzlyak, M. N. (1996). Use of a green channel in remote sensing of global vegetation from EOS-MODIS. *Remote Sensing of Environment, 58*(3), 289-298. https://doi.org/10.1016/S0034-4257(96)00072-7

Griffiths, S., Simmonds, J., Leverington, M., Wang, Y., Fish, L., Sayers, L., Alibert, L., Orford, S., Wingen, L., & Snape, J. (2012). Meta-QTL analysis of the genetic control of crop height in elite European winter wheat germplasm. *Molecular Breeding, 29*, 159-171. https://doi.org/10.1007/s11032-010-9534-x

Hagen, I., Huggel, C., Ramajo, L., Chacón, N., Ometto, J. P., Postigo, J. C., & Castellanos, E. J. (2022). Climate change-related risks and adaptation potential in Central and South America during the 21st century. *Environmental Research Letters, 17*(3), Article 033002. https://doi.org/10.1088/1748-9326/ac5271

Hall, A. J., & Richards, R. A. (2013). Prognosis for genetic improvement of yield potential and water-limited yield of major grain crops. *Field Crops Research, 143*, 18-33. https://doi.org/10.1016/j.fcr.2012.05.014

Hassan, M. A., Yang, M., Fu, L., Rasheed, A., Zheng, B., Xia, X., Xiao, Y., & He, Z. (2019). Accuracy assessment of plant height using an unmanned aerial vehicle for quantitative genomic analysis in bread wheat. *Plant Methods, 15*, Article 37. https://doi.org/10.1186/s13007-019-0419-7

Huete, A. R. (1988). A soil-adjusted vegetation index (SAVI). *Remote Sensing of Environment, 25*(3), 295-309. https://doi.org/10.1016/0034-4257(88)90106-X

Instituto Meteorológico Nacional. (2023). *El clima y las regiones climáticas de Costa Rica*. https://www.imn.ac.cr/documents/10179/31165/clima-regiones-climat.pdf/cb3b55c3-f358-495a-b66c-90e677e35f57

Jiang, Q., Fang, S., Peng, Y., Gong, Y., Zhu, R., Wu, X., Ma, Y., Duan, B., & Liu, J. (2019). UAV-based biomass estimation for rice-combining spectral, TIN-based structural and meteorological features. *Remote Sensing, 11*(7), Article 890. https://doi.org/10.3390/rs11070890

Jiang, Z., Tu, H., Bai, B., Yang, C., Zhao, B., Guo, Z., Liu, Q., Zhao, H., Yang, W., Xiong, L., & Zhang, J. (2021). Combining UAV-RGB high-throughput field phenotyping and genome-wide association study to reveal genetic variation of rice germplasms in dynamic response to drought stress. *New Phytologist, 232*(1), 440-455. https://doi.org/10.1111/nph.17580

Jordan, C. F. (1969). Derivation of leaf-area index from quality of light on the forest floor. *Ecology, 50*(4), 663-666. https://doi.org/10.2307/1936256

Kanke, Y., Tubaña, B., Dalen, M., & Harrell, D. (2016). Evaluation of red and red-edge reflectance-based vegetation indices for rice biomass and grain yield prediction models in paddy fields. *Precision Agriculture, 17*(5), 507-530. https://doi.org/10.1007/s11119-016-9433-1

Kawashima, S., & Nakatani, M. (1998). An algorithm for estimating chlorophyll content in leaves using a video camera. *Annals of Botany, 81*(1), 49-54. https://doi.org/10.1006/anbo.1997.0544

Li, J., Shi, Y., Veeranampalayam-Sivakumar, A. N., & Schachtman, D. P. (2018). Elucidating sorghum biomass, nitrogen and chlorophyll contents with spectral and morphological traits derived from unmanned aircraft system. *Frontiers in Plant Science, 9*, Article 1406. https://doi.org/10.3389/fpls.2018.01406

Louhaichi, M., Borman, M. M., & Johnson, D. E. (2001). Spatially located platform and aerial photography for documentation of grazing impacts on wheat. *Geocarto International, 16*(1), 65-70. https://doi.org/10.1080/10106040108542184

Malambo, L., Popescu, S. C., Murray, S. C., Putman, E., Pugh, N. A., Horne, D. W., Richardson, G., Sheridan, R., Rooney, W. L., Avant, R., Vidrine, M., McCutchen, B., Baltensperger, D., & Bishop, M. (2018). Multitemporal field-based plant height estimation using 3D point clouds generated from small unmanned aerial systems high-resolution imagery. *International Journal of Applied Earth Observation and Geoinformation, 64*, 31-42. https://doi.org/10.1016/j.jag.2017.08.014

Mandal, S., Bhattacharya, S., & Paul, S. (2022). Assessing the impact of coal-fired thermal power plant emissions on surrounding vegetation health using geoinformatics: a case study. *Safety in Extreme Environments, 4*, 81-100. https://doi.org/10.1007/s42797-022-00054-4

Marques Ramos, A. P., Prado Osco, L., Garcia Furuya, D. E., Nunes Gonçalves, W., Cordeiro Santana, D., Ribeiro Teodoro, L. P., Da Silva Junior, C. A., Capristo-Silva, G. F., Li, J., Rojo Baio, F. H., Marcato Junior, J., Teodoro, P. E., & Pistori, H. (2020). A random forest ranking approach to predict yield in maize with UAV-based vegetation spectral indices. *Computers and Electronics in Agriculture, 178*, Article 105791. https://doi.org/10.1016/j.compag.2020.105791

Matias, F. I., Caraza-Harter, M. V., & Endelman, J. B. (2020). FIELDimageR: An R package to analyze orthomosaic images from agricultural field trials. *The Plant Phenome Journal, 3*, Article e20005. https://doi.org/10.1002/ppj2.20005

Mbaye, M., Ndour, A., Gano, B., Dembele, J. S. B., Luquet, D., Beurier, G., & Audebert, A. (2022). UAV method based on multispectral imaging for field phenotyping. En N. A. Kane, D. Foncéka, & T. J. Dalton (Eds.), *Crop adaptation and improvement for drought-prone environments* (pp. 173-187). New Prairie Press. https://newprairiepress.org/ebooks/49/

Mesas-Carrascosa, F. J., Torres-Sánchez, J., Clavero-Rumbao, I., García-Ferrer, A., Peña, J.-M., Borra-Serrano, I., & López-Granados, F. (2015). Assessing optimal flight parameters for generating accurate multispectral orthomosaics by UAV to support site-specific crop management. *Remote Sensing, 7*(10), 12793-12814. https://doi.org/10.3390/rs71012793

Navure Team. (n. d.). Navure (2.7.1): *A data-science-statistic oriented application for making evidence-based decisions*. Retrieved December 4, 2024, from https://www.navure.com/download/

Orozco Barrantes, E., & Sánchez Ledezma, W. (2018). Evaluación de variedades e híbridos de sorgo forrajero en condiciones de Bosque Húmedo Tropical. *Alcances Tecnológicos, 8*(1), 45-54. https://doi.org/10.35486/at.v8i1.78

Peroni Venancio, L., Chartuni Mantovani, E., Do Amaral, C. H., Usher Neale, C. M., Zution Gonçalves, I., Filgueiras, R., & Coelho Eugenio, F. (2020). Potential of using spectral vegetation indices for corn green biomass estimation based on their relationship with the photosynthetic vegetation sub-pixel fraction. *Agricultural Water Management, 236*, Article 106155. https://doi.org/10.1016/j.agwat.2020.106155

Pix4D. (2017). *Pix4Dmapper4.1 User manual*. Retrieved August 20, 2023, from https://support.pix4d.com/hc/en-us/articles/204272989

Ranđelović, P., Đorđević, V., Miladinović, J., Prodanović, S., Ćeran, M., & Vollmann, J. (2023). High-throughput phenotyping for non-destructive estimation of soybean fresh biomass using a machine learning model and temporal UAV data. *Plant Methods, 19*, Article 89. https://doi.org/10.1186/s13007-023-01054-6

R Core Team. (2020). *R: A language and environment for statistical computing*. R Foundation for Statistical Computing. https://www.R-project.org

Rodriguez, O. (2023). *regressoR: Regression Data Analysis System*. R package version 3.0.2. https://CRAN.R-project.org/package=regressoR

Roujean, J. L., & Breon, F. M. (1995). Estimating PAR absorbed by vegetation from bidirectional reflectance measurements. *Remote Sensing of Environment, 51*(3), 375-384. https://doi.org/10.1016/0034-4257(94)00114-3

Rouse, J. W., Haas, R. H., Schell, J. A., & Deering, D.W. (1974, December 10-14). Monitoring vegetation systems in the Great Plains with ERTS. In National Aeronautics and Space Administration (Ed.), *Proceedings of the Third Earth Resources Technology Satellite (ERTS) Symposium* (NASA SP-351, Vol. 1, pp. 309-317). National Aeronautics and Space Administration.

Shi, Y., Thomasson, J. A., Murray, S. C., Pugh, N. A., Rooney, W. L., Shafian, S., Rajan, N., Rouze, G., Morgan, C. L. S., Neely, H. L., Rana, A., Bagavathiannan, M. V., Henrickson, J., Bowden, E., Valasek, J., Olsenholler, J., Bishop, M. P., Sheridan, R., Putman, E. B., … Yang, C. (2016). Unmanned aerial vehicles for high-throughput phenotyping and agronomic research. *PLOS One, 11*(7), Article e0159781. https://doi.org/10.1371/journal.pone.0159781

Shu, M., Li, Q., Ghafoor, A., Zhu, J., Li, B., & Ma, Y. (2023). Using the plant height and canopy coverage to estimation maize aboveground biomass with UAV digital images. *European Journal of Agronomy, 151*, Article 126957. https://doi.org/10.1016/j.eja.2023.126957

Stavrakoudis, D., Katsantonis, D., Kadoglidou, K., Kalaitzidis, A., & Gitas, I. Z. (2019). Estimating rice agronomic traits using drone-collected multispectral imagery. *Remote Sensing, 11*(5), Article 545. https://doi.org/10.3390/rs11050545

Tayade, R., Yoon, J., Lay, L., Khan, A. L., Yoon, Y., & Kim, Y. (2022). Utilization of spectral indices for high-throughput phenotyping. *Plants, 11*(13), Article 1712. https://doi.org/10.3390/plants11131712

United Nations. (2017, June 21). *World population projected to reach 9.8 billion in 2050, and 11.2 billion in 2100*. Retrieved November 20, 2023, from https://www.un.org/en/desa/world-population-projected-reach-98-billion-2050-and-112-billion-2100

Varela, S., Pederson, T., Bernacchi, C. J., & Leakey, A. D. B. (2021). Understanding growth dynamics and yield prediction of sorghum using high temporal resolution UAV imagery time series and machine learning. *Remote Sensing, 13*(9), Article 1763. https://doi.org/10.3390/rs13091763

Wan, L., Cen, H., Zhu, J., Zhang, J., Zhu, Y., Sun, D., Du, X., Zhai, L., Weng, H., Li, Y., Li, X., Bao, Y., Shou, J., & He, Y. (2020). Grain yield prediction of rice using multi-temporal UAV-based RGB and multispectral images and model transfer – a case study of small farmlands in the South of China. *Agricultural and Forest Meteorology, 291*, Article 108096. https://doi.org/10.1016/j.agrformet.2020.108096

Watanabe, K., Guo, W., Arai, K., Takanashi, H., Kajiya-Kanegae, H., Kobayashi, M., Yano, K., Tokunaga, T., Fujiwara, T., Tsutsumi, N., & Iwata, H. (2017). High-throughput phenotyping of sorghum plant height using an unmanned aerial vehicle and its application to genomic prediction modeling. *Frontiers in Plant Science, 8*, Article 421. https://doi.org/10.3389/fpls.2017.00421

Watt, M., Fiorani, F., Usadel, B., Rascher, U., Muller, O., & Schurr, U. (2020). Phenotyping: new windows into the plant for breeders. *Annual Review of Plant Biology, 71*, 689-712. https://doi.org/10.1146/annurev-arplant-042916-041124

Xie, Q., Dash, J., Huang, W., Peng, D., Qin, Q., Mortimer, H., Casa, R., Pignatti, S., Laneve, G., Pascucci, S., Dong, Y., & Ye, H. (2018). Vegetation indices combining the red and red-edge spectral information for leaf area index retrieval. *IEEE Journal of Selected Topics in Applied Earth Observations and Remote Sensing, 11*(5), 1482-1493. https://doi.org/10.1109/JSTARS.2018.2813281

Yang, G., Liu, J., Zhao, C., Li, Z., Huang, Y., Yu, H., Xu, B., Yang, X., Zhu, D., Zhang, X., Zhang, R., Feng, H., Zhao, X., Li, Z., Li, H., & Yang, H. (2017). Unmanned aerial vehicle remote sensing for field-based crop phenotyping: current status and perspectives. *Frontiers in Plant Science, 8*, Article 1111. https://doi.org/10.3389/fpls.2017.01111

Yue, J., Yang, G., Li, C., Li, Z., Wang, Y., Feng, H., & Xu, B. (2017). Estimation of winter wheat above-ground biomass using unmanned aerial vehicle-based snapshot hyperspectral sensor and crop height improved models. *Remote Sensing, 9*(7), Article 708. https://doi.org/10.3390/rs9070708

Zheng, H., Cheng, T., Zhou, M., Li, D., Yao, X., Tian, Y., Cao, W., & Zhu, Y. (2018). Improved estimation of rice aboveground biomass combining textural and spectral analysis of UAV imagery. *Precision Agriculture, 20*, 611-629. https://doi.org/10.1007/s11119-018-9600-7